Unraveling the eroded units of mountain belts using RSCM thermometry and cross-section balancing: example of the southwestern French Alps

Jocelyn Balansa, Abdeltif Lahfid, Jean-Claude Hippolyte, Nicolas Espurt, Pierre Henry, Séverine Caritg, Bertrand Fasentieux

Unraveling the eroded units of mountain belts using RSCM thermometry and cross-section balancing: example of the southwestern French Alps

Jocelyn Balansa[1], Abdeltif Lahfid[2,3], Nicolas Espurt[1,4], Jean-Claude Hippolyte[1], Pierre Henry[1], Séverine Caritg[2] and Bertrand Fasentieux[5]

[1]*Aix Marseille Univ, CNRS, IRD, INRAE, Coll France, CEREGE, Aix-en-Provence, France*

[2]*BRGM-French Geological Survey, Orléans, France*

[3]*UMR 7327 ISTO, Université d'Orléans, CNRS, BRGM, Orléans, France*

[4]*Université Côte d'Azur, CNRS, Observatoire de la Côte d'Azur, IRD, GEOAZUR, France*

[5]*Université de Pau et des Pays de l'Adour, E2S UPPA, CNRS, Total, LFCR, Pau, France*

Keywords

RSCM thermometry; Maximum temperature (T_{RSCM}); Balanced cross-section; Nappes; Burial; SW Alps

Abstract

Reconstruction of eroded mountain belt structures is crucial to produce valid pre-contractional palinspastic restorations and quantify the amount of shortening. In this study, we combine Raman Spectroscopy of Carbonaceous Material (RSCM) thermometry and cross-section balancing technique to propose a reconstruction of the thermal and deformational evolution of the Subalpine Digne Nappe in the southwestern French Alps. We sampled Mesozoic to Cenozoic sedimentary strata for RSCM thermometry analyses along the ~4-km-thick Digne Nappe to calculate maximum temperatures (T_{RSCM}). T_{RSCM} values range from 243±10°C to 349±13°C in the upper Triassic-upper Cretaceous strata and from 255±19°C to 328±8°C in the overlying upper Eocene-lower Oligocene strata. T_{RSCM} values show a gradual increase with depth and towards the inner part of the orogen. These results are consistent with a ~28±4°C/km modeled thermal gradient in the ~4-km-thick Digne Nappe

and suggest post Oligocene burial of the Digne Nappe under sedimentary/tectonic units that have been removed by erosion. Palinspastic restoration of a NE-trending and 65-km-long cross-section (Digne-Barcelonnette transect) constrained by thermal data supports the interpretation that the Digne Nappe involved a ~3-km-thick middle/upper Eocene-Oligocene to lower Miocene foreland basin tectonically overlain by the 3- to 11-km-thick Embrunais-Ubaye flysch nappes. The front of the Embrunais-Ubaye nappes was located ~40 km beyond its present erosional front. The amount of southwestward shortening in the Subalpine thrust wedge derived from palinspastic restoration is about 35 km (35%) over the past ~16 million years. Removal of a substantial volume of the southwestern Alpine orogen may have significantly influenced the dynamics of the Subalpine thrust wedge and Valensole foreland basin since the Middle Miocene.

Introduction

Orogenic wedges result from progressive horizontal transport and stacking of structural units formed by nappes and foreland basins (Elliott and Johnson 1980; Hardebol et al. 2009; Rosenberg et al. 2015). The uppermost structural units of these stacks may have been totally removed by erosion in the orogens (Malavieille 2010). A challenge is to quantify the volume of these missing units. The Alps represent a prime example of a modern collisional orogen whose structural evolution is still under debate (e.g., Dumont et al. 2022 and references therein). The Alpine orogen results from the subduction of the Eurasian continental margin (the Briançonnais domain) and the Piemont-Liguria Ocean beneath the Apulia microplate during the Cenozoic era (Kerckhove et al. 1974; Debelmas et al. 1983a; Michard et al. 2004; Dumont et al. 2012; Butler et al. 2013; van Hinsbergen et al. 2020). The Alpine thrust wedge is characterized by far-travelled stacked nappes that propagated toward the European foreland (Kerckhove et al. 1974; Bellahsen et al. 2014; Rosenberg et al. 2015). In the southwestern part of the Alpine wedge (Fig. 1), previous studies tried to constrain the

thickness of the eroded nappes from regional balanced and restored cross-sections (Debelmas et al. 1983a; Lickorish and Ford 1998; Graham et al. 2012) or thermal data (Corsini et al. 2004; Bigot-Cormier et al. 2006; Labaume et al. 2008; Cavailhes 2012; Bellanger et al. 2015; Rosenberg et al. 2021). These structural and thermal studies show strong variations in the restored nappe stack geometry and shortening. It raises the following questions: Where was the front of the nappes before erosion, and what was the thickness of these nappes? Here we study and reconstruct the thermal and tectonic history of the Subalpine Digne Nappe by combining maximum temperature data (T_{RSCM}), assessed through Raman Spectroscopy of Carbonaceous Material (RSCM) thermometry with cross-section balancing. The goal of this study is to reliably constrain the nature and geometry of the eroded structural units of the southwestern Alpine wedge and to quantify the burial of the sedimentary pile of the Digne Nappe. To illustrate the structure and kinematics of the southwestern Alpine nappe stack, we built a 65-km-long crustal-scale balanced cross-section across the northern edge of the Valensole basin, the Digne Nappe and the Embrunais-Ubaye nappes (Digne-Barcelonnette transect; Figs. 2, 3). We used geological and structural information from published geological maps and cross-sections (Goguel 1964; Kerckhove 1969; Gigot et al. 1974; Kerckhove et al. 1974; Arlhac et al. 1983; Debelmas et al., 1983a; Haccard et al. 1989a; Gidon and Pairis 1992; Balansa et al. 2022), and new field data.

Structure and kinematics of the southwestern Alpine nappe stack

The frontal thrust, the Subalpine Digne Nappe, is composed of a Mesozoic (upper Triassic to upper Cretaceous) sedimentary pile thickening northeastward from 2.2- to 4.5-km-thick (Digne basin), unconformably covered locally by up to 1.2-km-thick Eocene-Oligocene strata (composed of Lutetian “Argens conglomerates”, upper Eocene limestones and blue marls, lower Oligocene “Grès d’Annot”, and lower Oligocene “Schistes à Blocs” toward the hinterland; Figs. 3, 4, 5; Campredon 1972; Kerckhove et al. 1974; Arlhac et al. 1983; Rousset

et al. 1983; Ravenne et al. 1987; Haccard et al. 1989a; Sinclair 1997; Ford et al. 1999; Joseph et al. 2012). The inner part of the Digne Nappe, outcropping within the Barcelonnette window, reaches a maximum thickness of 2 km (Fig. 3; Kerckhove 1969; Debelmas et al. 1983a). The nappe is regionally detached southwesterly above middle-upper Triassic evaporites (Gidon and Pairis 1992). Shortening value reaches 22 km on its frontal part (Balansa et al. 2022). Lying at the footwall of the Digne Nappe, the Barles para-autochthonous unit involves a much thinner "Provençal" upper Carboniferous to lower Cretaceous sequence unconformably overlain by Cenozoic sediments filling the Valensole foreland basin (Gidon and Pairis 1992; Hippolyte et al. 2011; Schwartz et al. 2017; Balansa et al. 2022). The Barles para-autochthonous unit and the northern edge of the Valensole basin accommodate 10 km of shortening (Balansa et al. 2022). Hinterlandward, the Digne Nappe includes the imbricated thrust fan of the La Blanche Range (e.g., Dormillouse and Mandeysse units; Figs. 2, 3, 5; Goguel 1964; Kerckhove et al. 1978; Debelmas et al. 1983b; Hamiti 1994). Shortening of the Digne Nappe has been mainly fed from a basement thrust located under the Barcelonnette zone (Debelmas et al. 1983a; Michard et al. 2004; Lardeaux et al. 2006; Dumont et al. 2012). This basement thrust is interpreted as the northwestern continuation of the Argentera massif (Debelmas et al., 1983a; Fig. 1). Outer basement thrusts near Barles are active since the Early-Middle Miocene (Gigot et al. 1974; Haccard et al. 1989b; Graham et al. 2012; Balansa et al. 2022). After the emplacement of the Digne Nappe in Late Miocene-Pliocene, shortening in the Barles basement thrust wedge continued and was responsible for folding and erosion of the overlying Digne Nappe, which created the Barles half-window (Gigot et al. 1974; Schwartz et al. 2017; Balansa et al. 2022). These external basement thrusts could be connected northeastward at depth to the horizontal European lower crust as observed in the Cifalps transect (Malusà et al. 2021; Nouibat et al. 2022).

The inner Embrunais-Ubaye nappes form a broad klippe over the Subalpine Digne Nappe, preserved between the Argentera and Pelvoux Paleozoic massifs (Fig. 1). Equivalent nappes (San Remo-Monte Saccarello nappes) are found to the southeast of the Argentera Massif (Sanità et al. 2020). The Embrunais-Ubaye nappes include an upper thrust sheet, the Parpaillon Nappe and a lower thrust sheet, the Autapie Nappe (Kerckhove 1969; Figs. 2, 3, 6). They mainly consist of helminthoid flysch of Late Cretaceous to Paleocene age (Kerckhove 1969) locally involving basal tectonic slices of Briançonnais, Sub-Briançonnais and Digne Nappe units (upper Triassic to Eocene rocks; Fig. 6). The Embrunais-Ubaye flysch nappes originate from the Piemont-Liguria Ocean and their cumulate displacement is estimated to be >50 km (Kerckhove 1969; Merle and Brun 1984; Fry 1989; Ford et al. 1999). The initial thickness of the two Embrunais-Ubaye nappes is estimated between 5 and 10 km (Kerckhove 1969; Merle and Brun 1984; Hamiti 1994; Lickorish and Ford 1998; Corsini et al. 2004; Bigot-Cormier et al. 2006; Labaume et al. 2008; Cavailhes 2012). These nappes recorded an early northwestward thrusting in the Middle Eocene and a southwestward emplacement in the Early Oligocene associated with sedimentation of the Schistes à Blocs Formation (Kerckhove 1969; Merle and Brun 1984; Fry 1989; Dumont et al. 2012). The thrusting of the Parpaillon Nappe may have continued until the Early Miocene (Kerckhove 1969; Merle and Brun 1984; Fry 1989; Mark et al. 2016). Along the studied cross-section the erosional front is found along the northeastern slope of La Blanche Range immediately east of its imbricates (Figs. 2, 3, 5).

RSCM thermometry: methodology, sampling and results

The thermometric approach based on the carbonaceous material characterization using Raman spectroscopy tool provides the T_{RSCM} recorded by the rocks, quantitatively in the range 200°C to 650°C (e.g. Beyssac et al. 2002; Lahfid et al. 2010) and qualitatively in the range 100°C to 200°C (e.g. Lahfid et al. 2010; Saspiturry et al. 2020). RSCM thermometry

was successfully applied to track the thermal behavior in a large variety of geological settings (e.g., Labaume et al. 2016; Saspiturry et al. 2020; Girault et al. 2020; Caldera et al. 2020). RSCM thermometry analyses of this study were done at BRGM (French Geological Survey, Orléans) using a Renishaw inVia Reflex system and following the analysis procedure described in Lahfid et al. (2010). The Raman parameters of the defect bands in partially or entirely disordered carbonaceous materials depend on the energy of the incident laser radiation due to resonance effects (e.g., Ferrari and Robertson 2004). Thus, the laser source excitation was 514.5 nm (Lahfid et al. 2010). It was focused on the sample through a Leica DM2500 microscope using a x100 lens. To avoid heating damage in the ordered carbonaceous material structure, the laser beam power did not exceed 0.5 mW at the surface of the thin section. At least 10 spectra were recorded for each sample.

RSCM analyses were carried out on 34 samples from Mesozoic to Cenozoic slates and limestones of the Digne Nappe (Fig. 2; Table 1). Representative Raman spectra are shown in Fig. 7a. Samples at less than 10 km in horizontal distance to the cross-section have been projected onto the cross-section along the computed fold axes, i.e., 112°-2° axis in the La Robine zone and 319°-5° axis in the Seyne-Barcelonnette zone (Figs. 2, 3). Because the Digne Nappe is folded by the uplift of the Barles basement high, leading to variation along strike of height of the stratigraphic units, we projected the sample DIG20-28 with a dip of about 15° toward the southeast (Fig. 2). Samples have been collected far (>100 m in vertical distance) to major fault zones to avoid the effect of shear heating during thrust emplacement (Maino et al., 2015).

According to the shapes of Raman spectra carbonaceous materials obtained in this study, we used the RA1 Raman parameter proposed in Lahfid et al. (2010) to calculate T_{RSCM}. The RA1 parameter represents the relative area of D1 and D4 bands (area ratio RA1 = (D1 + D4) / (D1 + D2 + D3 + D4 + G)). T_{RSCM} were calculated using this equation:

$T_{RSCM} = 1217.6 \times RA1 - 450.66$

The fitting procedure followed to determine the band area is described in Lahfid et al. (2010) and is relatively similar to that given for the study of carbonaceous soots by Sadezky et al. (2005). This procedure represented in Fig. 7b consists in using a Lorentzian profile for all bands (G band and D1, D2, D3, D4 defect bands).

T_{RSCM} values range from 243±10°C to 349±13°C in the upper Triassic-Jurassic-upper Cretaceous sedimentary section and from 255±19°C to 328±8°C in the overlying upper Eocene-lower Oligocene sedimentary section (Figs. 2, 3, 4; Table 1). T_{RSCM} values show a gradual increase with depth and towards the inner part of the orogen. In the outer zones, the T_{RSCM} show a similar trend regarding the northeastward increase in temperature (from ~260°C in La Robine zone to ~330°C in Seyne area) compared to the increase in burial of the Jurassic section (Figs. 3, 8a). In the La Blanche Range imbricate, upper Eocene-lower Oligocene strata show a similar northeastward increase in T_{RSCM} value from 255°C to ~325°C (Figs. 2, 3, 5). In the Barcelonnette window, under the Embrunais-Ubaye nappes, we obtained T_{RSCM} values ranging from 281±11°C to 332±10°C in middle-upper Jurassic and lower Oligocene strata (Figs. 2, 4). Our T_{RSCM} values >240°C are in good agreement with widespread N130°-45°NE-dipping schistosity (normal to the southwestward compression trend) in the Mesozoic-lower Oligocene sedimentary pile of the Digne Nappe (Figs. 2, 4). This is also consistent with metamorphism grade evolution suggested by illite cristallinity index (semi quantitative analysis) and organic matter maturity data across the Mesozoic rocks of the Digne Nappe (Aprahamian 1988; Levert 1991; Hamiti 1994). Our data are also consistent with the T_{RSCM} values obtained by Bellanger et al. (2015) in Jurassic and Eocene-Oligocene sequences along the Embrunais valley and around the Pelvoux Massif (Fig. 1). Apatite fission-track (Labaume et al. 2008) and extensional fault zone fluid inclusions (Cavailhes 2012; Cavailhes et al. 2013, 2014) temperature data (~200-270°C) in the lower

Oligocene “Grès d’Annot” of the Digne Nappe (Restefond and Estrop areas; Fig. 2) are also close to our T_{RSCM} (255-281°C) in these zones.

Burial and geotherm estimation

T_{RSCM} reached in geological settings of low-grade metamorphism can be related to the effect of extensional/transtensional crustal deformation (i.e., crustal thinning during rifting associated with high thermal gradient) or compressional event (burial under thrust sheets and foreland basins associated with low thermal gradient) (e.g., Bellanger et al. 2015; Lahfid et al. 2019; Saspiturry et al. 2020; Caldera et al. 2020). Previous studies dealing with the thermal history of the Alps suggest that the Subalpine zone experienced heating during the Tethyan-Vocontian rifting then during the Oligocene-Miocene compression (Barlier et al. 1974; Levert 1991; Deville and Sassi 2006; Butler 2017). Recent tomographic data of the Cifalps transect (located ~30-35 km north of the Digne-Barcelonnette transect; Fig. 1) indicate that the European crust has a regular thickness of ~30 km below the Baronnies basin and the Digne Nappe (e.g., Nouibat et al. 2022). In this portion of the European crust, no thickness variation, which could support pre-contractional continental thinning with high thermal conditions, is observed. However, the 255±19°C-328±8°C T_{RSCM} recorded by the middle/upper Eocene-lower Oligocene cover of the Digne Nappe indicate that the entire sedimentary pile of the nappe attained its maximum temperature after the Early Oligocene (Figs. 2, 4, 5). This is consistent with previous studies in the western Alps suggesting that the Subalpine zone experienced burial/heating during the Oligocene-Miocene period (Deville and Sassi 2006; Bellanger et al. 2015). The increase of T_{RSCM} towards the internal part of the orogen (Fig. 3) is interpreted as resulting from tectonic burial under the Embrunais-Ubaye nappes and foreland sediments during the Oligocene-Miocene period. Therefore, we need now to define the thermal gradient to infer the thickness of the eroded pile above the Digne Nappe.

We performed a statistical model of T_{RSCM} within the Digne Nappe as a two-parameter linear regression of horizontal distance (D1) along the cross-section and depth (Z1) relative to the top of the Mesozoic for 25 samples localized southwest of the La Blanche Range (Fig. 8). In this eroded portion of the Digne Nappe, the top of the Mesozoic pile is estimated by southeasterly remnants of unconformable middle/upper Eocene-Oligocene strata and cross-section construction, assuming that the structural thickness of the Digne Nappe is similar to its initial stratigraphic thickness (Figs. 2, 3; Table 1). Our model approximates the temperature field within the Mesozoic-Cenozoic pile at the time of their maximum burial as a uniform geothermal gradient (temperature linearly increasing with Z1) combined with burial beneath a wedge of constant taper (temperature linearly increasing with D1). The regression parameters are calculated by weighted least square inversion, $1/SD^2$, where SD is the standard error on T_{RSCM} estimated for each sample. Error bounds on the regression parameters are given for a 95% confidence interval. If the effect of burial beneath the wedge is ignored, a simple linear regression $T_{RSCM}(Z1)$ may be applied but this yields a poor coefficient of determination $R^2=0.437$ and a low estimated gradient of 16±7°C/km (Fig. 8a). Fit of data is greatly improved in the two-parameter linear model (Fig. 8b). The coefficient of determination is $R^2=0.916$ and the best fit is:

$$T_{RSCM} = 174\pm15°C + 25\pm4°C/km \times Z1 + 2.1\pm0.4°C/km \times D1$$

The geothermal gradient is thus estimated to 25±4°C/km and the lateral gradient along the top of the Mesozoic is estimated to 2.1±0.4°C/km. The average taper of the wedge is given by the ratio of the lateral gradient and geothermal gradient, which is equal to 0.085 and corresponds to a 4.9° taper angle (an average value of the known taper angles of the modern orogens; e.g., Boyer 1995; Meigs and Burbank 1997). In Fig. 8b, the adjusted depth is calculated as:

$$Z = Z1 + 0.0857 \times D1$$

This adjustment accounts for burial beneath the wedge, and Z represents the depth beneath an arbitrary horizontal level (the depth of the top of the Mesozoic at D1=0). The estimated geothermal gradient represents the gradient within the Mesozoic-Cenozoic pile and thus at a depth of several kilometers. At equilibrium, the value determined by this method represents a lower bound to the average gradient between the surface and the samples because the radioactive heat production within the formation and the general increase of thermal conductivity with depth in sedimentary piles both contribute to decreasing gradient with depth. The consequences of the variation of conductivity with depth on the depth estimates remains small as this variation mostly occurs in the first 2 km where sediments are compacting. Moreover, it will mostly affect depth estimates near the toe of the wedge. However, the heat production in the bulk of a sediment wedge cannot be neglected. With the same parameters as in Goffé et al. (2003), heat conductivity 2.25 $W.m^{-1}.K^{-1}$ and radiogenic heat production 1 $\mu W.m^{-3}$, the average conductive gradient between the surface and a given depth z (in km) is 0.22×z °C/km above the conductive gradient at depth z. For instance, for a burial depth of 10 to 15 km, the average gradient from the surface is about 2 to 3°C/km above the gradient estimated at depth. This remains within uncertainties.

The calculated 25±4°C/km geothermal gradient at depth is coherent with a classical collisional-type gradient. It is consistent with orogen-scale numerical models, which show that for a slow convergence rate the geotherm within the frontal part of the orogenic wedge remains close to the initial geotherm assumed for the continent entering the orogen (for instance, with 4-8 mm/yr convergence rate as may be assumed for the Alps, see Bousquet et al. 1997). Assuming that the samples were affected by a similar post Oligocene burial history and taking into account radioactive heat production a geothermal gradient of 28±4°C/km should be considered as a reasonable average between the surface and depth to validate burial

estimations along the cross-section. Considering a mean surface temperature of 10°C, we estimate the burial depth of the samples between ~9 km to the foreland and ~11 km to the hinterland (Table 1).

Palinspastic restoration of the Digne Nappe and structural implications

The cross-section was restored and balanced using "MOVE" software on the basis of the flexural-slip algorithm, which allows to maintain bed lengths and areas (Dahlstrom 1969). Because the T_{RSCM} of the sedimentary pile was acquired after compaction, sediment decompaction was not performed (Nunns 1991). The burial estimation of each sample derived from T_{RSCM} and a 28±4°C/km geothermal gradient have been placed on the restored cross-section (Fig. 9a) to constrain the shape of the prism prior to thrusting into the Subalpine zone (Early-Middle Miocene, ~16Ma). The restored envelope surface is consistent with the present wedge geometry (Fig. 9b), considering the lowest elevation in the foreland and a progressive elevation increase toward the hinterland (~5° taper angle). The restoration illustrates the initial position and geometry of the basement outcropping in the Argentera massif, which along our cross-section was probably also a structural high initially uplifted during the Mesozoic before Cenozoic shortening and inversion. It is inferred from the restoration that the inner Embrunais-Ubaye nappes travelled far southwestward (~40 km of displacement ahead of its present erosional front) along a gently northeastward-dipping basal thrust fault (Fig. 9a). The geodynamic reconstruction arising from the model is a crustal flexure as a combination of tectonic load of the Embrunais-Ubaye nappes and sedimentary load of a middle/upper Eocene-Oligocene to lower Miocene foreland basin (Fig. 9a). The T_{RSCM} preserved in the hinterland by Mesozoic-lower Oligocene sedimentary section are interpreted as mainly resulting from tectonic burial under the Embrunais-Ubaye nappes. According to the cross-section restoration and T_{RSCM} data, these nappes have exceeded 11 km in thickness in the hinterland (Fig. 9a). The thickest tectonic unit was the Parpaillon Nappe.

The nappe stack thinned toward the foreland, from 5- to 3-km-thick. An additional ~3-km-thick ~50 km-wide, northeastward-dipping foreland basin is required to explain the observed T_{RSCM} in the underlying Mesozoic-Paleogene sequence of the future Digne Nappe (Fig. 9a). The restoration and the present thickness data suggest that the basin was composed of at least 1.3-km-thick middle/upper Eocene-lower Oligocene strata and the rest by upper Oligocene and lower Miocene strata. This early Alpine flexural foreland basin is the response to Alpine thickening and loading in the southwestern Alps between the Middle/Late Eocene and the Early Miocene. The Embrunais-Ubaye nappes propagated southwestward in this depression between the Argentera and Pelvoux structural highs during the Middle-Late Miocene (Merle and Brun 1984; Dumont et al. 2012). Thus, a now mainly eroded large middle/upper Eocene-Oligocene to lower Miocene foreland basin existed in the southwestern Alps along the study transect like that still present in the northwestern Alps (Girault et al. 2022). Cross-section restoration also suggests that the Jurassic strata of the Barles unit (footwall of the future Digne Nappe) have been buried by only ~400- to 900-m-thick Oligocene-lower Miocene foreland strata. Although the T_{RSCM} recorded by the Jurassic strata of the Barles units is not constrained, the lack of schistosity (excepted along localized fault zones), that contrasts with the pervasive schistosity in the Digne Nappe (Hamiti 1994), suggests only shallow burial of the para-autochthonous during the Oligocene-Miocene.

According to T_{RSCM} data/burial depth estimations, the palinspastic restoration of the cross-section suggests a total horizontal crustal shortening of ~35 km (35%) for the Subalpine zone during the Middle Miocene to Present (Fig. 9). Approximately 26 km of this shortening were transferred into the Digne Nappe, the rest (9 km) into the Barles zone. We calculate a mean shortening rate, since ~16 Ma, of ~2.2 mm/yr for the Subalpine zone. These values are in accordance with the shortening values calculated by Balansa et al. (2022) for the frontal part of the Subalpine zone. The restoration also suggests that the La Blanche Range

imbricates and folds (Figs. 5 and 9b) in the footwall of the Embrunais-Ubaye nappes might have developed during the emplacement of the Embrunais-Ubaye nappes in the Late Oligocene-Early Miocene period. Although the La Blanche Range imbricate was not restored, its shortening is estimated greater than 7 km as suggested by Hamiti (1994).

Based on low-temperature apatite fission-track and (U-Th)/He data, Schwartz et al. (2017) confirmed that the northern edge of the Neogene Valensole basin and Barles unit located in the footwall of the Digne Nappe were heated up to ~100°C. For a mean geothermal gradient of 28°C/km and surface temperature of 10°C, these low-temperature thermochronology data are consistent with an upper Neogene tectonic burial of lower Miocene strata of the Valensole basin under the 3.3-km-thick Digne Nappe (Fig. 9b). This result suggests that erosion has removed a large thickness (>8 km) of the sedimentary/tectonic cover of the Digne Nappe in the Middle to Late Miocene.

Many geological and analog/numerical modeling studies showed that the dynamics of orogenic wedges is governed by complex interactions between deformation, erosion and sedimentation processes (e.g., Davis et al. 1983; Baby et al. 1995; Avouac and Burov 1996; Meigs and Burbank 1997; Bonnet al. 2008; Malavieille 2010; Fillon et al. 2013; Steer et al. 2014; Erdős et al. 2015; Butler 2020; Liu et al. 2020; Malavieille et al. 2021). For instance, the growth and uplift of an antiformal nappe stack can focus erosion in the internal zones. In turn, this localized erosion can favor internal deformation and the development of very active thrust accommodating large displacements (Bonnet et al. 2008). Based on our results along the Digne-Barcelonnette transect, we propose that the large erosional unloading of the inner Alpine wedge might have contributed to the rapid basement thrusting (Bigot-Cormier et al. 2006) and the large displacement of the Subalpine Digne Nappe in Middle-Late Neogene (Balansa et al. 2022). The erosion of the Embrunais-Ubaye/Digne nappe stack may have provided large sediment influx toward the foreland (paleo-Durance river), leading to the

formation of the Valensole basin in this segment of the Alpine orogen. Similarly, the development of the Nice basin to the southeast could have been favored by the erosion of the San Remo-Monte Saccarello flysch nappes (Fig. 1). However, the eroded volume of these nappes is not yet constrained.

Conclusion

In the southwestern French Alps along the Digne-Barcelonnette transect, the ~4-km-thick Mesozoic-Cenozoic sedimentary pile of the Subalpine Digne Nappe records T_{RSCM} ranging from 243±10°C to 349±13°C, resulting from substantial burial in a typical ~28±4°C/km orogenic geotherm. We proposed a structural model in which the Digne Nappe has been overburdened under the 3- to 11-km-thick inner Embrunais-Ubaye nappe wedge and ~3-km-thick frontal middle/upper Eocene-lower Miocene foreland basin. The leading edge of the Embrunais-Ubaye nappes is estimated ~40 km ahead of its present erosional front. Cross-section restoration indicates that ~35 km (35%) of horizontal crustal shortening were accommodated in the Subalpine zone over the past ~16 million years, which implies a shortening rate of ~2.2 mm/yr. The removal of substantial units of the southwestern Alpine orogen might have significantly unloaded the wedge, which has undeniably influenced the Subalpine thrust wedge propagation since the Middle Miocene.

Acknowledgments

This project has been supported by the BRGM-RGF (French Geological Survey-Référentiel Géologique de la France) Alpes et bassins périphériques program. We thank Myette Guiomar from the Réserve Naturelle Géologique de Haute-Provence for field assistance. Cross-section balancing was performed using the MOVE Software Suite donated by Petroleum Experts Limited. Diagrams of Fig. 2 have been performed using Stereonet v. 11 by R.W. Allmendinger.

References

Aprahamian J (1988) Cartographie du métamorphisme faible à très faible dans les Alpes françaises externes par l'utilisation de la cristallinité de l'illite. Geodinamica Acta 2:1:25-32. https://doi:10.1080/09853111.1988.11105153

Arlhac P, Beaudoin B, Kerckhove C, Rouire J, Rousset C (1983) Carte géologique de la France (1/50000), Feuille Seyne (894). Orléans. Bureau de Recherches Géologiques et Minières.

Avouac JP, Burov EB (1996) Erosion as a driving mechanism of intracontinental mountain growth. J Geophys Res Solid Earth 101 B8:17747-17769. https://doi.org/10.1029/96JB01344

Baby P, Colletta B, Zubieta D (1995) Etude géométrique et expérimentale d'un bassin transporté : exemple du synclinorium de l'Alto Beni (Andes centrales). Bull Soc géol Fr 166 6:797-811

Balansa J, Espurt N, Hippolyte JC, Philip J, Caritg S (2020) Structural evolution of the superimposed Provençal and Subalpine fold-thrust belts (SE France). Earth-Science Reviews 227:103972. https://doi.org/10.1016/j.earscirev.2022.103972

Barlier J, Ragot JP, Touray JC (1974) L'évolution des Terres Noires subalpines méridionales d'après l'analyse minéralogique des argiles et la réflectométrie des particules carbonées. Bulletin du BRGM 6:533-548

Bellahsen N, Mouthereau F, Boutoux A, Bellanger M, Lacombe O, Jolivet L, Rolland Y (2014) Collision kinematics in the western external Alps Tectonics 33:1055-1088. https://doi:10.1002/2013TC003453

Bellanger M, Augier R, Bellahsen N, Jolivert L, Monié P, Baudin T, Beyssac O (2015) Shortening of the European Dauphinois margin (Oisans Massif, Western Alps): New

insights from RSCM maximum temperature estimates and $^{40}Ar/^{39}Ar$ in situ dating. Journal of Geodynamics 83:37-64. http://dx.doi.org/10.1016/j.jog.2014.09.004

Beyssac O, Goffé B, Chopin C, Rouzaud JN (2002) Raman spectra of carbonaceous material in metasediments: a new geothermometer. Journal of Metamorphic Geology 20:859-871. https://doi:10.1046/j.1525-1314.2002.00408.x

Bigot-Cormier F, Sosson M, Poupeau G, Stéphan JF, Labrin E. (2006) The denudation history of the Argentera Alpine External Crystalline Massif (Western Alps, France-Italy): an overview from the analysis of fission tracks in apatites and zircons. Geodinamica Acta 19:6:455-473. https://doi:10.3166/ga.19.455-473

Bonnet C, Malavieille J, Mosar J (2008) Surface processes versus kinematics of thrust belts: impact on rates of erosion, sedimentation, and exhumation - Insights from analogue models. Bull Soc géol Fr 179:297-314. https://doi.org/10.2113/gssgfbull.179.3.297

Bousquet R, Goffé B, Henry P, Le Pichon X, Chopin C (1997) Kinematic, thermal and petrological model of the Central Alps: Lepontine metamorphism in the upper crust and eclogitisation of the lower crust. Tectonophysics 273:105-127, https://doi:10.1016/S0040-1951(96)00290-9

Boyer SE (1995) Sedimentary basin taper as a factor controlling the geometry and advance of thrust belts. American Journal of Science 295:1220-1254. https://doi:10.2475/ajs.295.10.1220

Butler RWH (2013) Area balancing as a test of models for the deep structure of mountain belts, with specific reference to the Alps. Journal of Structural Geology 52:2-16. https://doi.org/10.1016/j.jsg.2013.03.009

Butler RWH (2017) Basement-cover tectonics, structural inheritance, and deformation migration in the outer parts of orogenic belts: A view from the western Alps, Linkages and Feedbacks in Orogenic Systems, RD Law, JR Thigpen, AJ Merschat,

HH Stowell. Geological Society of America Memoirs 213. https://doi.org/10.1130/2017.1213(03)

Butler RWH (2020) Syn-kinematic strata influence the structural evolution of emergent fold–thrust belts. In: Hammerstein JA, Di Cuia R, Cottam MA, Zamora G, Butler RWH (Eds.). Fold and Thrust Belts: Structural Style, Evolution and Exploration. Geological Society London Special Publications 490:57-78. https://doi.org/10.1144/SP490-2019-14

Caldera N, Teixell A, Griera A, Labaume P, Lahfid A (2021) Recumbent folding in the Upper Cretaceous Eaux-Chaudes massif: a Helvetic-type nappe in the Pyrenees? Terra Nova 33:320-331. https://doi:10.1111/ter.12517

Campredon R (1972) Les formations paléogènes des Alpes maritimes franco-italiennes. PhD Thesis, Université Nice Sophia Antipolis. 2 vol., 539p. tel-00801742

Cavailhes T (2012) Architecture et propriétées pétrophysiques des zones de failles dans une série gréso-pélitique profondément enfouie : rôle de la déformation et des interactions fluide-roche. Exemple des Grés d'Annot (France). Phd Thesis, Université Montpellier 2, 397p. tel-01310382

Cavailhes T, Sizun JP, Labaume P, Chauvet A, Buatier M, Soliva R, Mezri L, Charpentier D, Leclère H, Travé A, Gout C (2013) Influence of fault rock foliation on fault zone permeability: The case of deeply buried arkosic sandstones (Grès d'Annot, southeastern France). AAPG Bulletin 97:1521-1543. https://doi:10.1306/03071312127

Cavailhes T, Labaume P, Sizun JP, Soliva R, Gout C, Potdevin JL, Buatier M, Gay A, Chauvet A, Charpentier D, Travé A (2014) Difference in petrophysical properties between foliated and dilatant fault rocks in deeply buried clastics: The case of the

Grès d'Annot Formation, SW French Alps. TerraNova 26:298-306, https://doi: 10.1111/ter.12100

Corsini M, Ruffet G, Caby R (2004) Alpine and late-hercynian geochronological constraints in the Argentera Massif (Western Alps). Eclogae geol Helv 97:3-15. https://doi.org/10.1007/s00015-004-1107-8

Dahlstrom CDA (1969) Balanced cross-sections. Canadian Journal of Earth Sciences 6:743-757. https://doi:10.1139/e69-069

Davis D, Suppe J, Dahlen FA (1983) Mechanics of fold-and-thrust belts and accretionary wedges. J Geophys Res Solid Earth 88 B2:11531172. https://doi.org/10.1029/JB088iB02p01153

Debelmas J, Escher A, Trumpy R (1983a) Profiles through the western Alps. In: Profiles of orogenic belts. Geodyn Ser, Am Geophys Union 10:83-96

Debelmas J, Arnaud H, Gidon M, Kerckhove C, Giraud P, Lemoine M, Menot JP, Monjuvent G, Vialon P (1983b) Guides géologiques régionaux: Alpes du Dauphiné. France Masson (Ed) 198 p

Deville E, Sassi W (2006) Contrasting thermal evolution of thrust systems: An analytical and modeling approach in the front of the western Alps. AAPG Bulletin 90:887-907. https://doi:10.1306/01090605046

Dumont T, Schwartz S, Guillot S, Malusà M, Jouvent M, Monié P, Verly A (2022) Cross-propagation of the western Alpine orogen from early to late deformation stages: Evidence from the Internal Zones and implications for restoration. Earth-Science Reviews 232:104106. https://doi.org/10.1016/j.earscirev.2022.104106

Dumont T, Schwartz S, Guillot S, Simon-Labric T, Tricart P, Jourdan S (2012) Structural and sedimentary records of the Oligocene revolution in the Western Alpine arc. Journal of Geodynamics 56-57:18-38. https://doi:10.1016/j.jog.2011.11.006

Elliott D, Johnson MRW (1980) Structural evolution in the northern part of the Moine thrust Zone, NW Scotland. Transactions of the Royal Society, Edinburgh 71:69-96

Erdős Z, Huismans RS, van der Beek P (2015). First-order control of syntectonic sedimentation on crustal-scale structure of mountain belts. J Geophys Res Solid Earth 120:5362-5377. https://doi.org/10.1002/2014JB011785

Fillon C, Huismans RS, van der Beek P (2013) Syntectonic sedimentation effects on the growth of fold-and-thrust belts. Geology 41:83-86. https://doi.org/10.1130/G33531.1

Ferrari AC, Robertson J (2004) Raman spectroscopy of amorphous, nanostructured, diamond–like carbon, and nanodiamond. Philosophical Transactions of the Royal Society of London. Series A: Mathematical, Physical and Engineering Sciences 362 1824:2477-2512. https://doi.org/10.1098/rsta.2004.1452

Ford M, Lickorish WH, Kusznir NJ (1999) Tertiary foreland sedimentation in the Southern Subalpine Chains, SE France: a geodynamic appraisal. Basin Res 11:315-336. https://doi.org/10.1046/j.1365-2117.1999.00103.x

Fry N (1989) Southwestward thrusting tectonics of the western Alps. In: Alpine Tectonics (Ed. By MP Coward, D Dietrich and RG Park), Geol Soc London Spec Publ 45:83-109

GEOL-ALP. http://www.geol-alp.com by Maurine Gidon, 1998-2019.

Gidon M, Pairis JL (1992) Relations entre le charriage de la Nappe de Digne et la structure de son autochtone dans la vallée du Bès (Alpes de Haute-Provence, France). Eclogae Geologicae Helvetiae 85/2:327-359

Gigot P, Grandjacquet C, Haccard D (1974) Evolution tectono-sédimentaire de la bordure septentrionale du bassin tertiaire de Digne depuis l'Eocène. Bulletin de la Société Géologique de France 7 XVI 2:128-139. https://doi.org/10.2113/gssgfbull.S7-XVI.2.128

Girault JB, Bellahsen N, Boutoux A, Rosenberg CL, Nanni U, Verlaguet A, Beyssac O (2020) The 3-D thermal Structure of the Helvetic Nappes of the European Alps: Implications for Collisional Processes. Tectonics 39. https://doi:10.1029/2018TC005334

Girault JB, Bellahsen N, Bernet M, Pik R, Loget N, Lasseur E, Rosenberg CL, Balvay M, Sonnet M (2022) Exhumation of the Western Alpine collisional wedge: New thermochronological data. Tectonophysics 822. https://doi:10.1016/j.tecto.2021.229155

Goffé B, Bousquet R, Henry P, Le Pichon X (2003) Effect of the chemical composition of the crust on the metamorphic evolution of orogenic wedges. Journal of Metamorphic Geology 21:123-141. https://doi.org/10.1046/j.1525-1314.2003.00422.x

Goguel J (1964) Duplicatures de la crête de la Blanche près Seyne (Basses-Alpes). Bulletin de la Société Géologique de France 7 VI:28-35. https://doi.org/10.2113/gssgfbull.S7-VI.1.28

Graham R, Jackson M, Pilcher R, Kilsdonk B (2012) Allochthonous salt in the sub-Alpine fold-thrust belt of Haute Provence, France, in Alsop GI, Archer SG, Hartley AJ, Grant NT, Hodgkinson R, eds., Salt Tectonics, Sediments and Prospectivity. Geological Society, London, Special Publications 363:595-615. https://doi:10.1144/SP363.30

Haccard D, Beaudoin B, Gigot P, Jorda M, et al. (1989a) Carte géologique de la France (1/50 000), Feuille La Javie (918). Orléans: Bureau de Recherches Géologiques et Minières.

Haccard D, Beaudoin B, Gigot P, Jorda M (1989b) Notice explicative, Carte géol. Fr. (1/50 000), feuille LA JAVIE (918). Orléans : Bureau de recherches géologiques et minières.

Hamiti M (1994) Géometrie, cinématique et mécanismes des chevauchements synschisteux dans une région préalablement déformée. Exemple de la couverture sédimentaire à

l'ouest du massif de l'Argentera (Alpes occidentales françaises). Phd Thesis. Aix-Marseille III, 195p. tel-01949169

Hardebol NJ, Callot JP, Bertotti G, Faure JL (2009) Burial and temperature evolution in thrust belt systems: Sedimentary and thrust sheet loading in the SE Canadian Cordillera. Tectonics 28:TC3003. https://doi:10.1029/2008TC002335

Hippolyte JC, Clauzon G, Suc JP (2011) Messinian-Zanclean canyons in the Digne nappe (southwestern Alps): tectonic implications. Bulletin de la Société Géologique de France 182 :111-132. https://doi:10.2113/gssgfbull.182.2.111

Joseph P, Callec Y, Ford, M (2012) Dynamic Controls on Sedimentology and Reservoir Architecture in the Alpine Foreland Basin. A Field Guide to the Eocene-Oligocene Grès d'Annot Turbidite System of the SE France, IFP Energies Nouvelles e-books, 128p. https://doi:10.2156/ifpen/2012001

Kerckhove C (1969) La Zone du flysch dans les nappes de l'Embrunais-Ubaye (Alpes Occidentales), Ph.D. thesis. Géologie appliquée. Université Joseph-Fourier-Grenoble I 205p

Kerckhove C, Pairis JL, Plan J, Schneegans D (1974) Carte géologique de la France (1/50 000), Feuille Barcelonnette (895). Orléans: Bureau de Recherches Géologiques et Minières

Kerckhove C, Debelmas J, Cochonat P (1978) Tectonique de soubassement parautochtone des nappes de l'Embrunais-Ubaye sur leur bordure occidentale, du Drac au Verdon. Géologie Alpine 54:67-82

Labaume P, Jolivet M, Souquière F., Chauvet A (2008) Tectonic control on diagenesis in a foreland basin: combined petrologic and thermochronologic approaches in the Grès d'Annot basin (Late Eocene-Early Oligocene, French-Italian external Alps). Terra Nova 20:95-101. https://doi:10.1111/j.1365-3121.2008.00793.x

Labaume P, Meresse F, Jolivet M, Teixell A, Lahfid A (2016) Tectonothermal history of an exhumed thrust-sheet-top basin: An example from the south Pyrenean thrust belt. Tectonics 35:1280-1313. https://doi:10.1002/2016TC004192

Lahfid A, Beyssac O, Deville E, Negro F, Chopin C, Goffé B (2010) Evolution of the Raman spectrum of carbonaceous material in low-grade metasediments of the Glarus Alps (Switzerland). Terra Nova 22:354-360. https://doi:10.1111/j.1365-3121.2010.00956.x

Lahfid A, Baidder L, Ouanaimi H, Soulaimani A, Hoepffner C, Farah A, Saddiqi O, Michard A (2019) From extension to compression: high geothermal gradient during the earliest Variscan phase of the Moroccan Meseta; a first structural and RSCM thermometric study. European Journal of Mineralogy 31. https://doi:10.1127/ejm/2019/0031-2882

Lardeaux JM, Schwartz S, Tricart P, Paul A, Guillot S, Béthoux N, Masson F (2006) A crustal-scale cross-section of the south-western Alps combining geophysical and geological imagery. Terra Nova 18:412-422. https://doi: 10.1111/j.1365-3121.2006.00706.x

Levert J (1991) Répartition géographique des minéraux argileux dans les sédiments mésozoïques du bassin subalpin : mise en évidence d'une diagenèse complexe. Phd Thesis. Documents des Laboratoires de Géologie, Lyon 114 175p

Lickorish WH, Ford M (1998) Sequential restoration of the external Alpine Digne thrust system, SE France, constrained by kinematic data and synorogenic sediments, in Mascle A et al., eds., Cenozoic Foreland Basins of Western Europe. Geological Society of London Special Publication 134:189-211. https://doi:10.1144/GSL.SP.1998.134.01.09

Liu Y, Tan X, Ye Y, Zhou C, Lu R, Murphy MA, Xu X, Suppe J (2020) Role of erosion in creating thrust recesses in a critical-taper wedge: An example from Eastern Tibet.

Earth and Planetary Science Letters 54:116270. https://doi.org/10.1016/j.epsl.2020.116270

Maino M, Casini L, Ceriani A, Decarlis A, Di Giulio A, Seno S, Setti M, Stuart FM (2015) Dating shallow thrusts with zircon (U-Th)/He thermochronometry-The shear heating connection. Geology 3:495-498. https://doi:10.1130/G36492.1

Malavieille J (2010) Impact of erosion, sedimentation, and structural heritage on the structure and kinematics of orogenic wedges: Analog models and case studies. GSA Today 20: 4-10. https://doi:10.1130/GSATG48A.1

Malavieille J, Dominguez S, Lu CY, Chen CT, Konstantinovskaya E (2021) Deformation partitioning in mountain belts: insights from analogue modelling experiments and the Taiwan collisional orogen. Geological Magazine 158:84-103. https://doi:10.1017/S0016756819000645

Malusà MG, Guillot S, Zhao L, Paul A, Solarino S, Dumont T, Schwartz S, Aubert C, Baccheschi P, Eva E, Lu Y, Lyu C, Pondrelli S, Salimbeni S, Sun W, Yuan H (2021) The deep structure of the Alps based on the CIFALPS seismic experiment: A synthesis. Geochemistry, Geophysics, Geosystems 22:e2020GC009466. https:// doi.org/10.1029/2020GC009466

Mark J, Cogné N, Chew D (2016) Tracking exhumation and drainage divide migration of the Western Alps: A test of the apatite U-Pb thermochronometer as a detrital provenance tool. GSA Bulletin 128:1439-1460. https://doi: 10.1130/B31351.1

Meigs AJ, Burbank DW (1997) Growth of the south Pyrenean orogenic wedge. Tectonics 16:239-258. https://doi:10.1029/96TC03641

Merle O, Brun JP (1984) The curved translation path of the Parpaillon Nappe (French Alps). Journal of Structural Geology 6:711-719. https://doi.org/10.1016/0191-8141(84)90010-5

Michard A, Avigad D, Goffé B, Chopin C (2004) The high-pressure metamorphic front of the south Western Alps (Ubaye-Maira transect, France, Italy). Schweizerische Mineralogische und Petrographische Mitteilungen 84:215-235

Nouibat A, Stehly L, Paul A, Schwartz S, Bodin T, Dumont T, Rolland Y, Brossier R, Cifalps Team and AlpArray Working Group (2022) Lithospheric transdimensional ambient-noise tomography of W-Europe: implications for crustal-scale geometry of the W-Alps. Geophys J Int 229:862-879. https://doi.org/10.1093/gji/ggab520

Nunns AG (1991) Structural restoration of seismic and geologic sections in extensional regimes. AAPG Bulletin 75:278-297. https://doi:10.1306/0C9B27A9-1710-11D7-8645000102C1865D

Ravenne C, Riché P, Trémolières P, Vially R (1987) Sedimentation and Tectonics in the Upper Eocene-Oligocene Marine Basin in the Southern Alps. Oil & Gas Science and Technology Rev. IFP 42:529-553. https://doi.org/10.2516/ogst:1987031

Rosenberg CL, Berger A, Bellahsen N, Bousquet R (2015) Relating orogen width to shortening, erosion, and exhumation during Alpine collision. Tectonics 34:1306-1328. https://doi:10.1002/2014TC003736

Rosenberg C, Bellahsen N, Rabaute A, Girault JB (2021) Distribution, style, amount of collisional shortening, and their link to Barrovian metamorphism in the European Alps. Earth-Science Reviews 222:103774. https://10.1016/j.earscirev.2021.103774

Rousset C, Kerckhove C, Bambier A (1983) Notice explicative, Carte géol. Fr. (1/50000), feuille SEYNE (894). Bureau de recherches géologiques et minières, Orléans

Sadezky A, Muckenhuder H, Grothe H, Niessner R, Pöschl U (2005) Raman microspectroscopy of soot and related carbonaceous materials: Spectral analysis and structural information. Carbon 43 8:1731-1742. https://doi.org/10.1016/j.carbon.2005.02.018

Sanità E, Lardeaux JM, Marroni M, Gosso G, Pandolfi L (2020) Structural relationships between Helminthoid Flysch and Briançonnais Units in the Marguareis Massif: A key for deciphering the finite strain pattern in the external southwestern Alps. Geological Journal 56:2024-2040. https://doi.org/10.1002/gj.4040

Saspiturry N, Lahfid A, Baudin T, Guillou- Frottier L, Razin P, Issautier B, Le Bayon B, Serrano O, Lagabrielle Y, Corre B (2020) Paleogeothermal gradients across an inverted hyperextended rift system: Example of the Mauléon fossil rift (Western Pyrenees). Tectonics 39. https://doi:10.1029/2020TC006206

Schwartz S, Gautheron C, Audin L, Dumont T, Nomade J, Barbarand J, Pinna-Jamme R, van der Beek P (2017) Foreland exhumation controlled by crustal thickening in the Western Alps. Geology 45:139-142. https://doi:10.1130/G38561.1

Sinclair HD (1997) Tectono-stratigraphic model for underfilled peripheral foreland basins: an alpine perspective. Geological Society of America Bulletin 109:324-346. https://doi.org/10.1130/0016-7606(1997)109<0324:TMFUPF>2.3.CO;2

Steer P, Simoes M, Cattin R, Shyu JBH (2014) Erosion influences the seis-micity of active thrust faults. Nat Commun 5:5564. https://doi.org/10.1038/ncomms6564

Van Hinsbergen DJ, Torsvik TH, Schmid SM, Matenco LC, Maffione M, Vissers RLM, Gürer D, Spakman W (2020) Orogenic architecture of the Mediterranean region and kinematic reconstruction of its tectonic evolution since the Triassic. Gondwana Research 81:79-229. https://doi:10.1016/j.gr.2019.07.009

Figure captions

Fig. 1 Geodynamic setting of the southwestern Alps. Black frame: study area (Fig. 2). Dashed black line: Digne-Barcelonnette balanced cross-section (Fig. 3). Dashed white line: crustal-scale Cifalps profile.

Fig. 2 (a) Simplified structural map of the study area (modified from Kerckhove et al. 1974; Arlhac et al. 1983; Haccard et al. 1989a) showing RSCM samples with T_{RSCM} (°C). The locations of the Digne-Barcelonnette balanced cross-section of Fig. 3 and surficial cross-section of Fig. 5 are shown. Field photographs of Figs. 4 and 6 are also shown. (b) The direction of the Digne-Barcelonnette balanced cross-section is chosen using the mean great circle analysis of bedding plane poles (points). The cross-section has two distinct trends: N22° in the La Robine zone and ~N49° in the Seyne-Barcelonnette zone. Mean fold axes (squares) are used to project RSCM samples onto the cross-section. (c) Schistosity planes measured in the Digne Nappe. Bedding poles and schistosity planes have been projected in a Schmidt diagram, lower hemisphere. Cgts: Conglomerates. SB: Schistes à Blocs.

Fig. 3 Balanced cross-section with projected location of the RSCM samples with T_{RSCM} (°C). See location in Fig. 2. Samples have been projected according to mean fold axes, i.e., 112°-2° axis in the La Robine zone and 319°-5° axis in the Seyne-Barcelonnette zone (see Fig. 2). Bedding traces are indicated by thin black lines. Cgts: Conglomerates. SB: Schistes à Blocs.

Fig. 4 Field photographs of sampled rocks for RSCM analyses in the Digne Nappe. T_{RSCM} data are indicated by red numbers. See locations in Fig. 2. (a) Toarcian slates along the Auzet-Seyne road (sample DIG20-39). (b) Upper Cretaceous limestones unconformably covered by upper Eocene limestones in the lower Ubaye valley (samples UBA21-6A and UBA21-6B). (c) Lower Oligocene "Grès d'Annot" under the Embrunais-Ubaye nappes in the lower Ubaye valley (sample UBA20-2; see location also in Fig. 6). (d) Callovian-Oxfordian "Black shales" in the Barcelonnette half-window (sample UBA20-10).

Fig. 5 Surficial cross-section showing the present front of the Autapie Nappe above the La Blanche Range imbricates (here the Dormillouse and Mandeysse units) in the lower Ubaye valley. See location in Fig. 2. This is a composite cross-section using previous cross-sections

from Goguel (1964), Kerckhove et al. (1978), Debelmas et al. (1983b) and GEOL-ALP website from M. Gidon.

Fig. 6 (a) Panoramic view of the superimposed Parpaillon Nappe, Autapie Nappe and Digne Nappe (Mandeysse tectonic slice) in the Ubaye River (44.447070°, 6.401534°; see location in Fig. 2). A 319±11°C T_{RSCM} is measured in lower Oligocene "Grès d'Annot" (sample UBA20-2; see details in Fig. 4c).

Fig. 7 (a) Selection of representative Raman spectra of carbonaceous materials and the corresponding temperatures (±20°C) in the Digne Nappe (see Table 1). G: Graphite band. D: Defect band. To avoid polishing effect, Raman analyses have been performed on carbonaceous materials covered by transparent minerals as revealed here by carbonate peaks. (b) Peak-fitting of the Raman spectrum of disordered carbonaceous material from DIG 20-3 sample. This spectrum is composed of a G band and D1, D2, D3, D4 defect bands (see Sadezky et al. 2005 for band labelling). For peak-fitting, each of the five bands has a pure Lorentzian shape and no a priori restriction is imposed on the band position, FWHM or relative intensity.

Fig. 8 Thermal modeling of the Digne Nappe. (a) Simple linear regression of the T_{RSCM}. (b) Improved two-parameter linear model of the T_{RSCM}. See details of parameters in Table 1 and explanations in text.

Fig. 9 Restored cross-sections of the southwestern Alpine orogenic wedge (see location in Fig. 2). The restoration is constrained with thickness estimations of the eroded units according to T_{RSCM} data and 28±4°C/km geothermal gradient (see Table 1). (a) The palinspastic restoration at ~16 Ma shows the volume of eroded units of the southwestern Alpine nappe stack with the 3- to 11-km-thick Embrunais-Ubaye nappe wedge associated with a ~3-km-thick ~50-km-wide foreland basin. (b) Present state with restoration of the

eroded Digne Nappe envelope. The thickness of the Digne Nappe above the northern edge of the Valensole basin (Barles tectonic half-window) was ~3.3 km (see more details in the text). Same legend as Figure 3. Bedding traces are indicated by thin black lines. BR: La Blanche Range imbricates

Table 1 Sample locations and ages, Raman spectroscopy of carbonaceous material data, and thermal modeling data of the Digne Nappe. The Raman parameter used to estimate temperatures is the RA1 from Lahfid et al. (2010). Raman parameter and T_{RSCM} are expressed in terms of mean values and SD (standard deviation) of all the data obtained for each sample. Standard errors (SE) are given for all the temperatures (SD divided by the square root of the number of measurements). D1: Distance along the cross-section. Z1: Depth below top of Mesozoic strata. Depth estimations are calculated for a 28±4°C/km geothermal gradient (see Fig. 8) and a surface temperature of 10°C

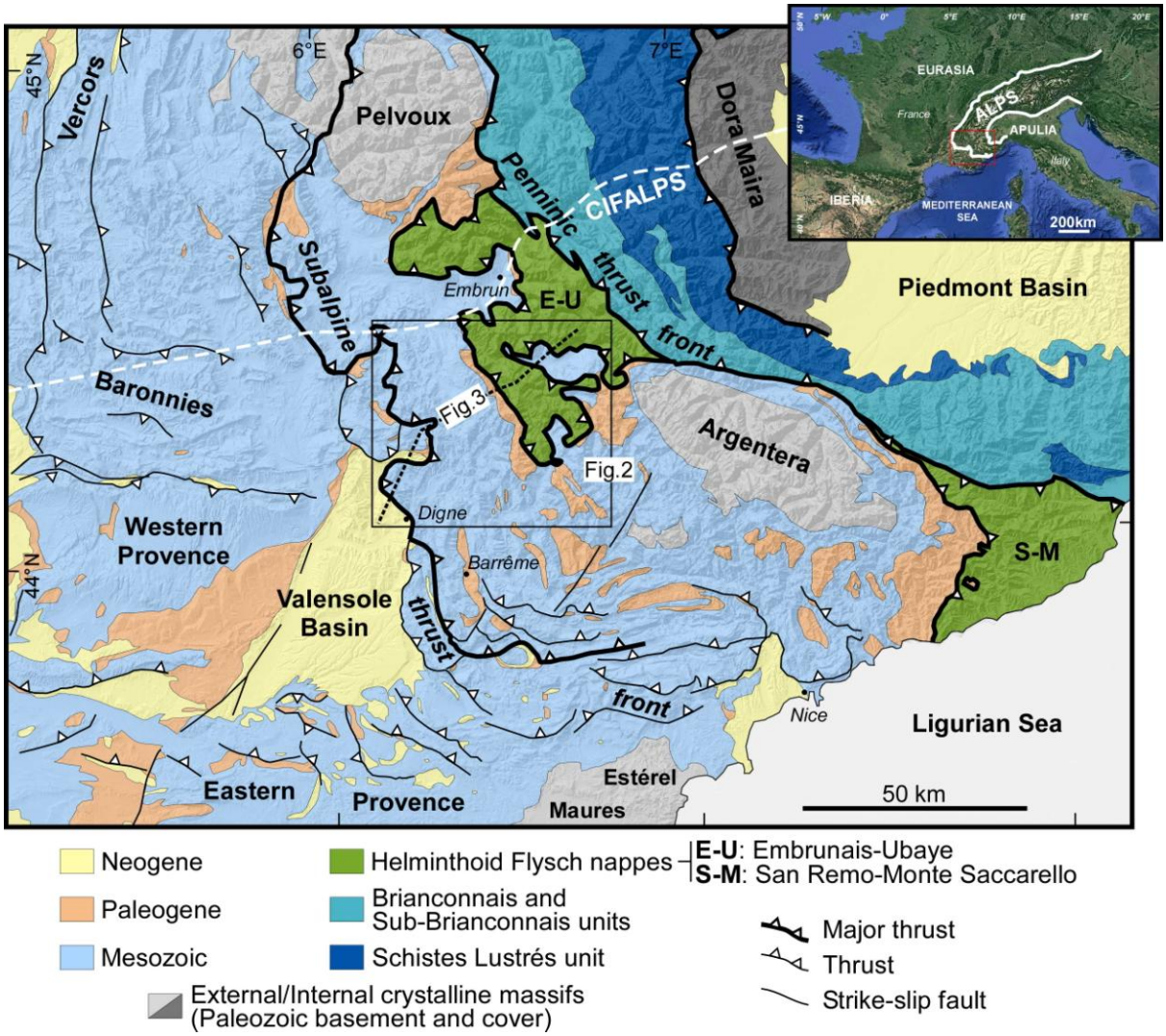
6°E
7°E
45°N
44°N
Vercors
Pelvoux
Dora Maira
Penninic thrust front
CIFALPS
Subalpine
Embrun
E-U
Piedmont Basin
Baronnies
Fig.3
Fig.2
Argentera
Digne
Western Provence
Barrême
S-M
Valensole Basin
thrust
front
Nice
Ligurian Sea
Eastern
Provence
Estérel
Maures
50 km
EURASIA
ALPS
France
APULIA
Italy
IBERIA
MEDITERRANEAN SEA
200km
Neogene
Paleogene
Mesozoic
Helminthoid Flysch nappes
Brianconnais and Sub-Brianconnais units
Schistes Lustrés unit
External/Internal crystalline massifs (Paleozoic basement and cover)
E-U: Embrunais-Ubaye
S-M: San Remo-Monte Saccarello
Major thrust
Thrust
Strike-slip fault

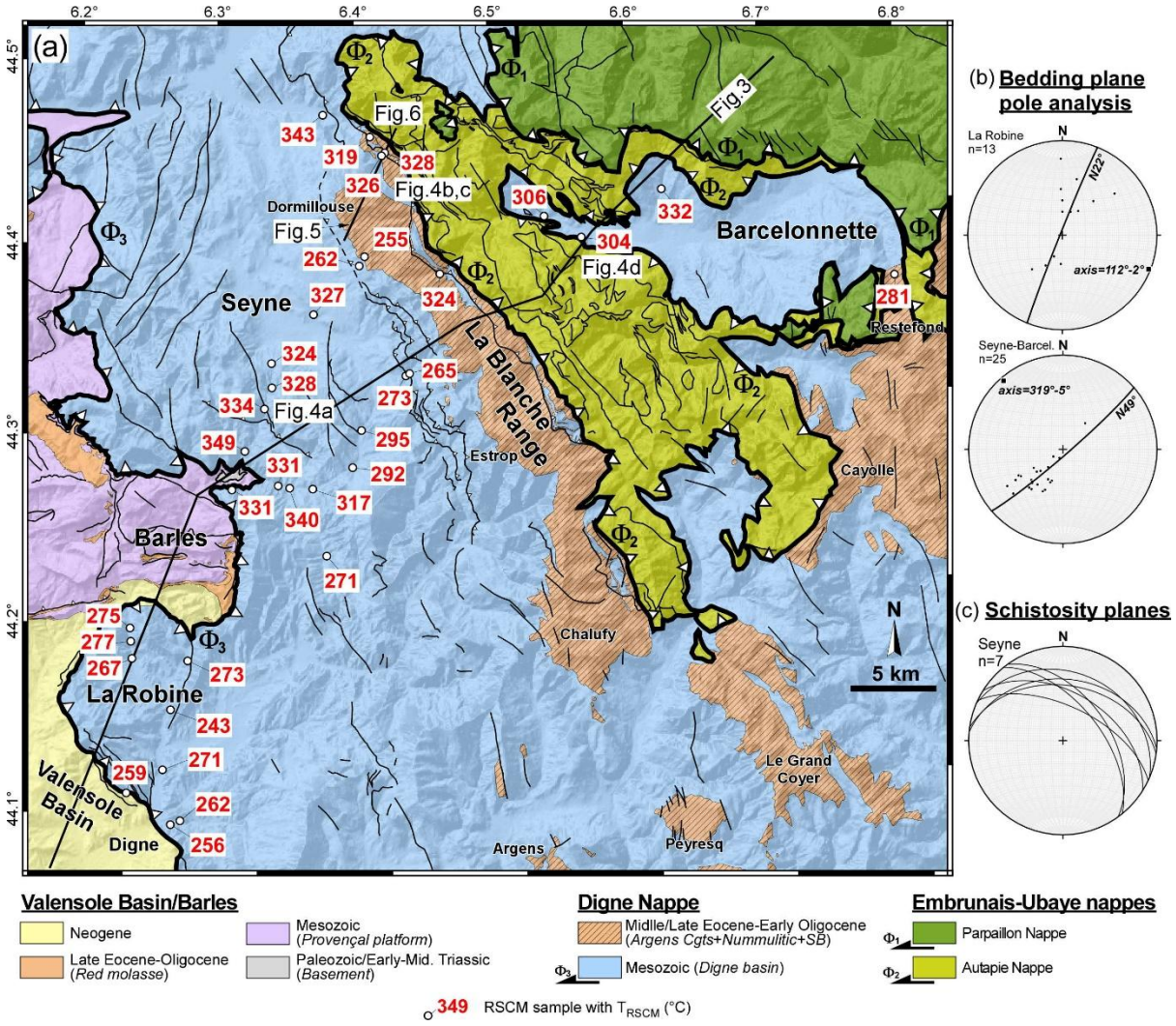
(a)
6.2°
6.3°
6.4°
6.5°
6.6°
6.7°
6.8°
44.5°
44.4°
44.3°
44.2°
44.1°
Fig.6
Fig.3
Fig.4b,c
Fig.5
Fig.4d
Fig.4a
Dormillouse
Seyne
Barcelonnette
Restefond
La Blanche Range
Estrop
Cayolle
Barles
Chalufy
La Robine
Valensole Basin
Digne
Argens
Peyresq
Le Grand Coyer
5 km
343
319
328
326
306
332
255
262
304
281
327
324
265
324
328
334
273
349
295
331
292
331
317
340
271
275
277
267
273
243
271
259
262
256
(b) Bedding plane pole analysis
La Robine n=13
axis=112°-2°
N22°
Seyne-Barcel. n=25
axis=319°-5°
N49°
(c) Schistosity planes
Seyne n=7
Valensole Basin/Barles
Neogene
Late Eocene-Oligocene (Red molasse)
Mesozoic (Provençal platform)
Paleozoic/Early-Mid. Triassic (Basement)
Digne Nappe
Midlle/Late Eocene-Early Oligocene (Argens Cgts+Nummulitic+SB)
Mesozoic (Digne basin)
Embrunais-Ubaye nappes
Parpaillon Nappe
Autapie Nappe
349 RSCM sample with T RSCM (°C)

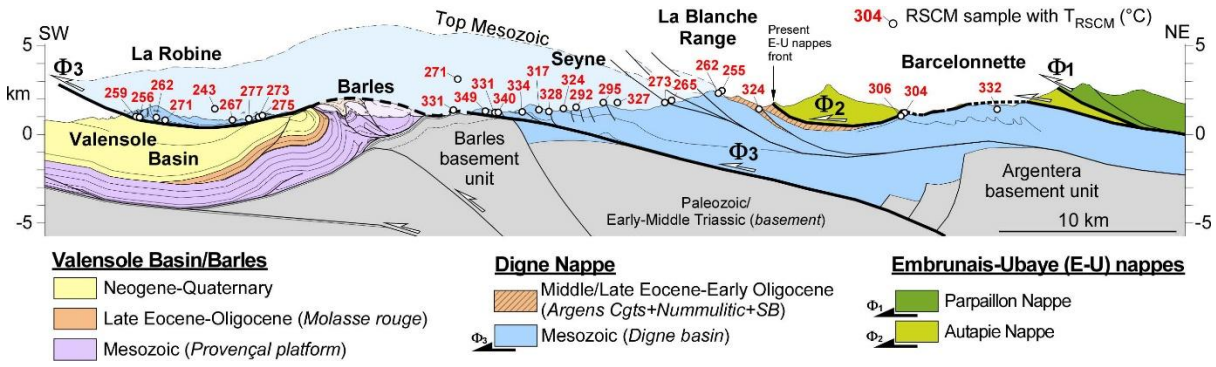
SW
NE
5
km
0
-5
Top Mesozoic
La Robine
Barles
Seyne
La Blanche Range
Present E-U nappes front
Barcelonnette
Φ3
Φ2
Φ1
Valensole Basin
Barles basement unit
Argentera basement unit
Paleozoic/ Early-Middle Triassic (basement)
10 km
304 RSCM sample with T RSCM (°C)
259 256 262 271 243 267 277 273 275
271 331 349 334 340 317 328 324 292 295 327
273 265 262 255 324
306 304 332
Valensole Basin/Barles
Neogene-Quaternary
Late Eocene-Oligocene (Molasse rouge)
Mesozoic (Provençal platform)
Digne Nappe
Middle/Late Eocene-Early Oligocene (Argens Cgts+Nummulitic+SB)
Mesozoic (Digne basin)
Embrunais-Ubaye (E-U) nappes
Parpaillon Nappe
Autapie Nappe

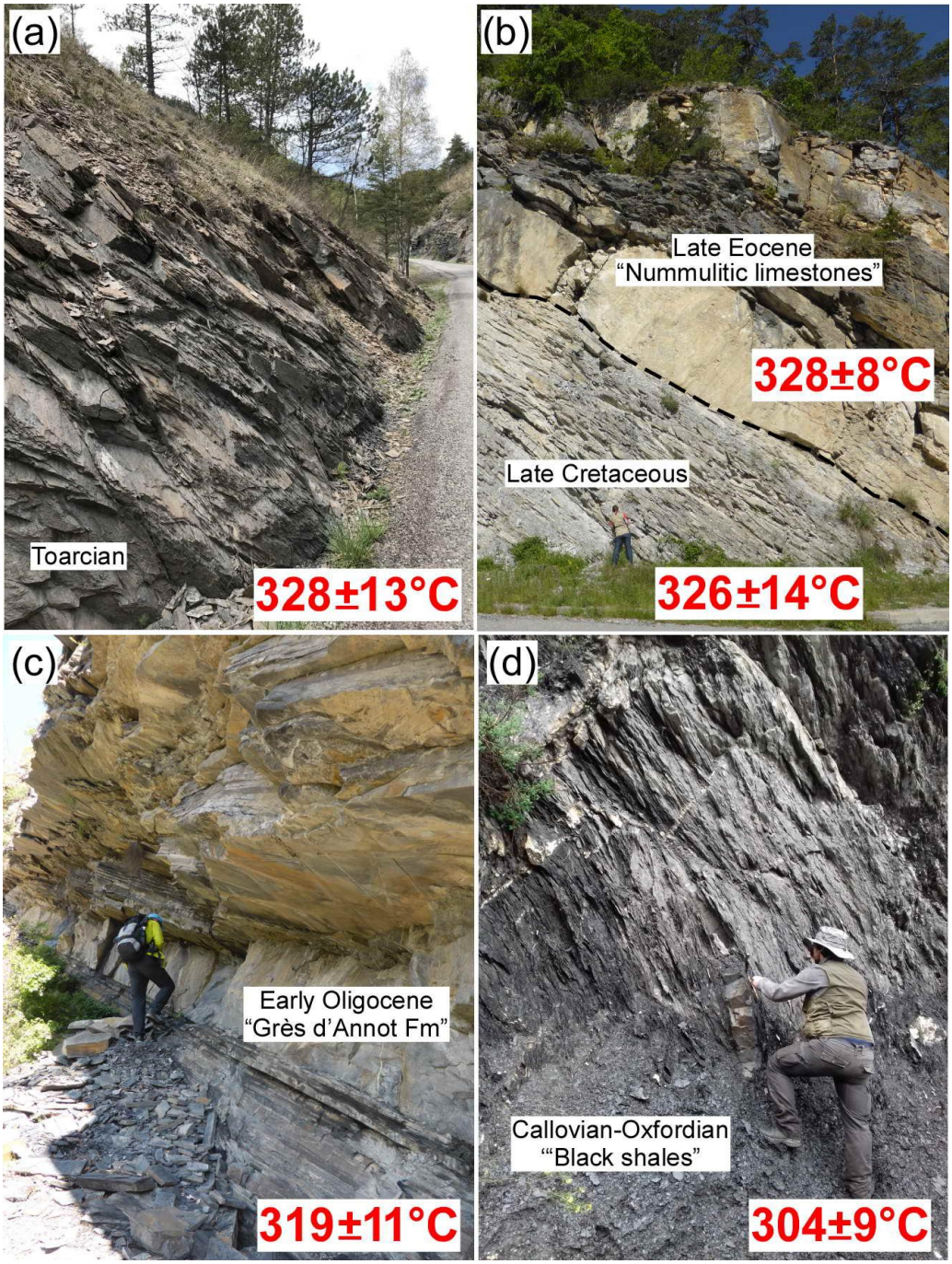
(a)
Toarcian
328±13°C
(b)
Late Eocene
"Nummulitic limestones"
328±8°C
Late Cretaceous
326±14°C
(c)
Early Oligocene
"Grès d'Annot Fm"
319±11°C
(d)
Callovian-Oxfordian
'"Black shales"
304±9°C

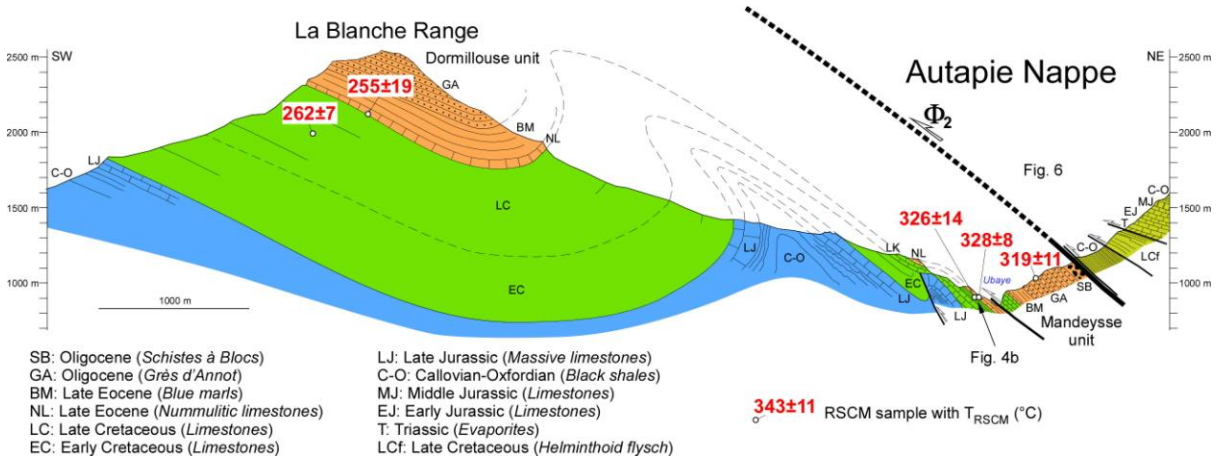
La Blanche Range
Autapie Nappe
SW
NE
2500 m
2000 m
1500 m
1000 m
Dormillouse unit
255±19
262±7
GA
BM
NL
LJ
C-O
LC
EC
1000 m
Φ2
Fig. 6
326±14
328±8
319±11
LK
MJ
EJ
T
LCf
SB
Ubaye
Mandeysse unit
Fig. 4b
SB: Oligocene (Schistes à Blocs)
GA: Oligocene (Grès d'Annot)
BM: Late Eocene (Blue marls)
NL: Late Eocene (Nummulitic limestones)
LC: Late Cretaceous (Limestones)
EC: Early Cretaceous (Limestones)
LJ: Late Jurassic (Massive limestones)
C-O: Callovian-Oxfordian (Black shales)
MJ: Middle Jurassic (Limestones)
EJ: Early Jurassic (Limestones)
T: Triassic (Evaporites)
LCf: Late Cretaceous (Helminthoid flysch)
343±11 RSCM sample with T RSCM (°C)

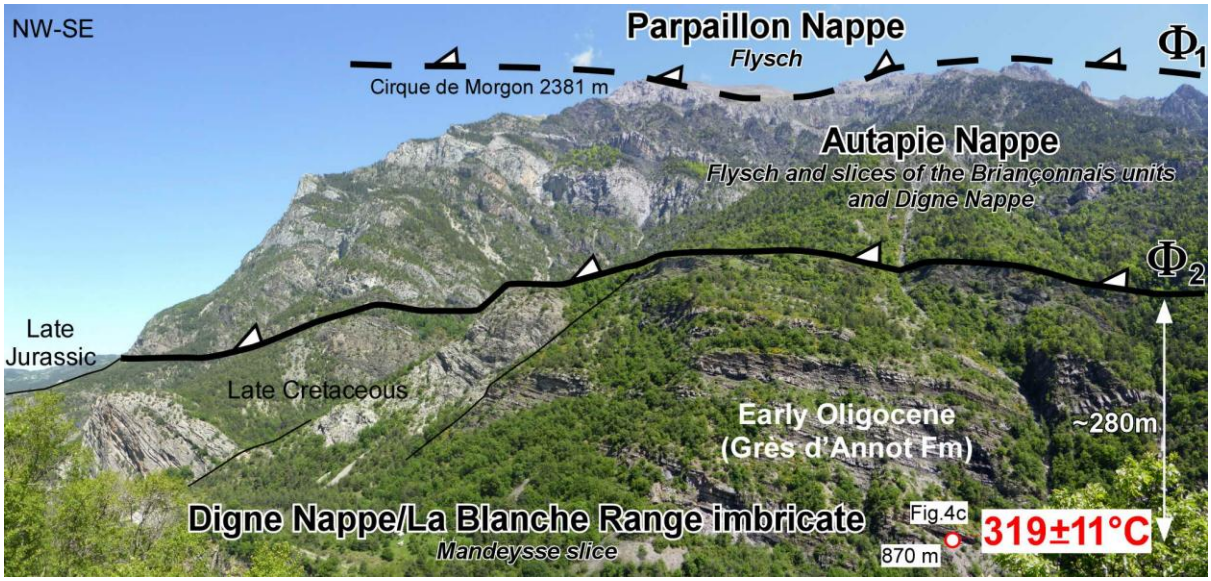
NW-SE
Parpaillon Nappe
Flysch
Φ1
Cirque de Morgon 2381 m
Autapie Nappe
Flysch and slices of the Briançonnais units and Digne Nappe
Φ2
Late Jurassic
Late Cretaceous
Early Oligocene
(Grès d'Annot Fm)
~280m
Digne Nappe/La Blanche Range imbricate
Mandeysse slice
Fig.4c
870 m
319±11°C

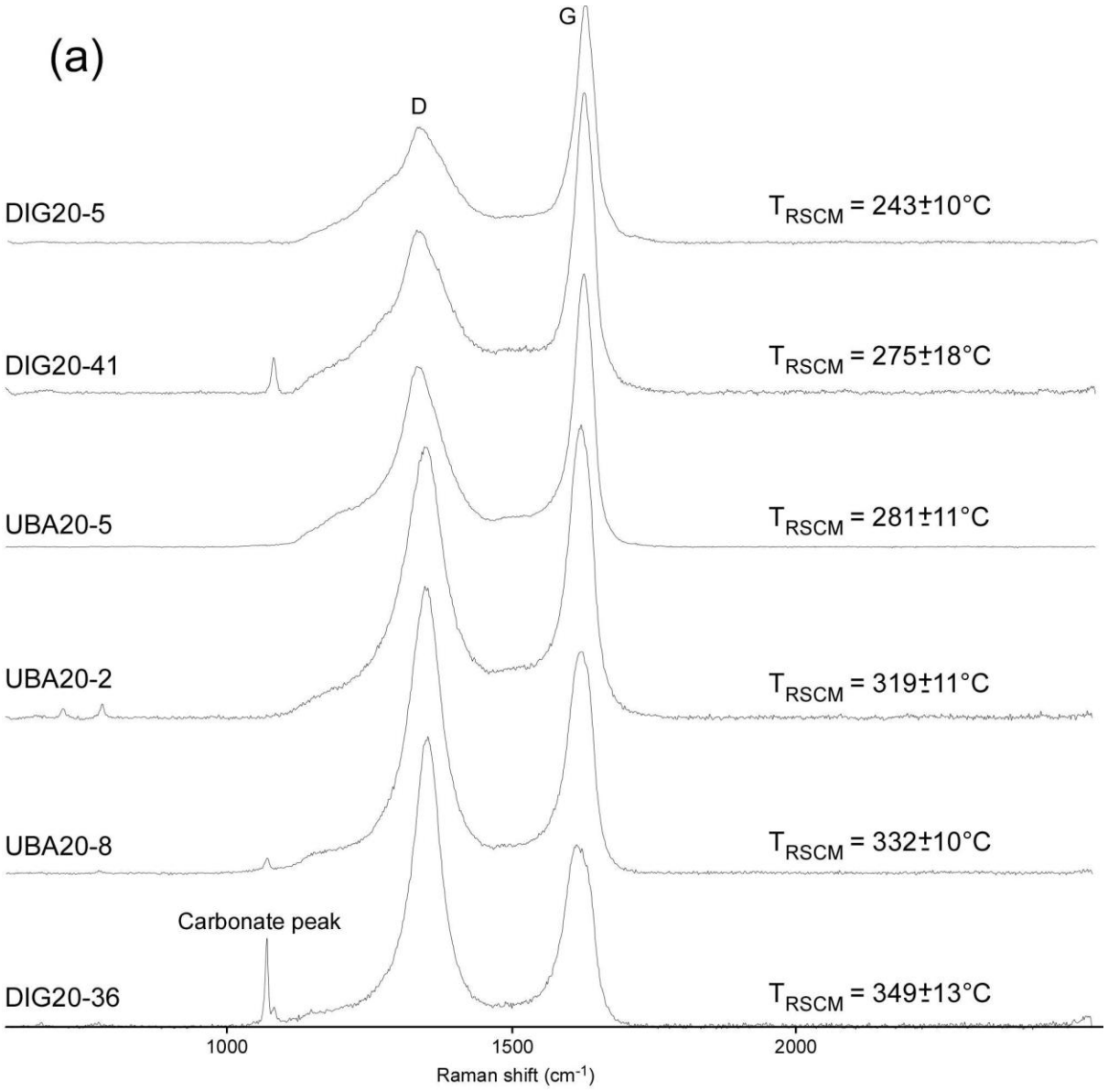
(a)
G
D
DIG20-5
T_{RSCM} = 243±10°C
DIG20-41
T_{RSCM} = 275±18°C
UBA20-5
T_{RSCM} = 281±11°C
UBA20-2
T_{RSCM} = 319±11°C
UBA20-8
T_{RSCM} = 332±10°C
Carbonate peak
DIG20-36
T_{RSCM} = 349±13°C
1000
1500
2000
Raman shift (cm^{-1})

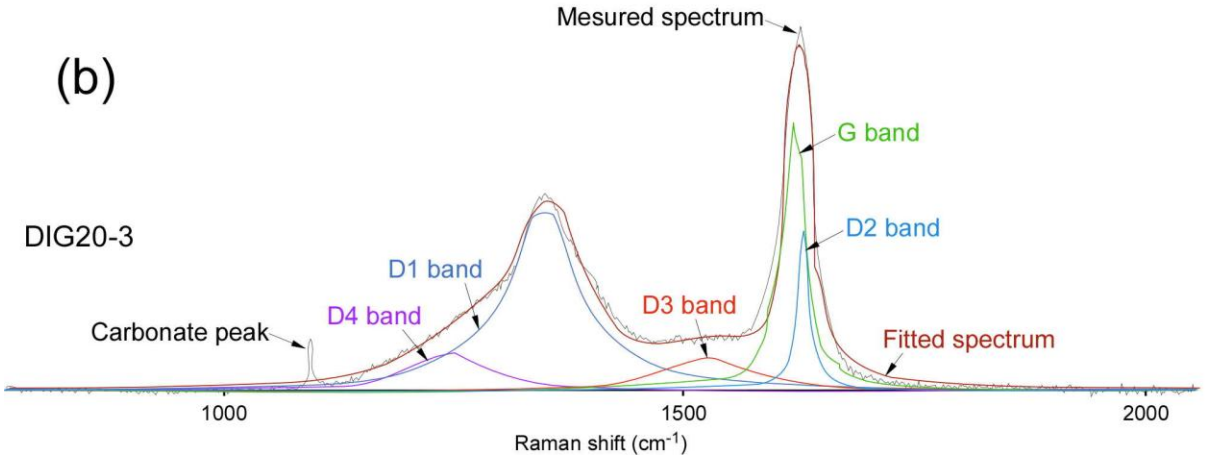
(b)
Mesured spectrum
G band
D2 band
DIG20-3
D1 band
D4 band
D3 band
Carbonate peak
Fitted spectrum
1000
1500
2000
Raman shift (cm^{-1})

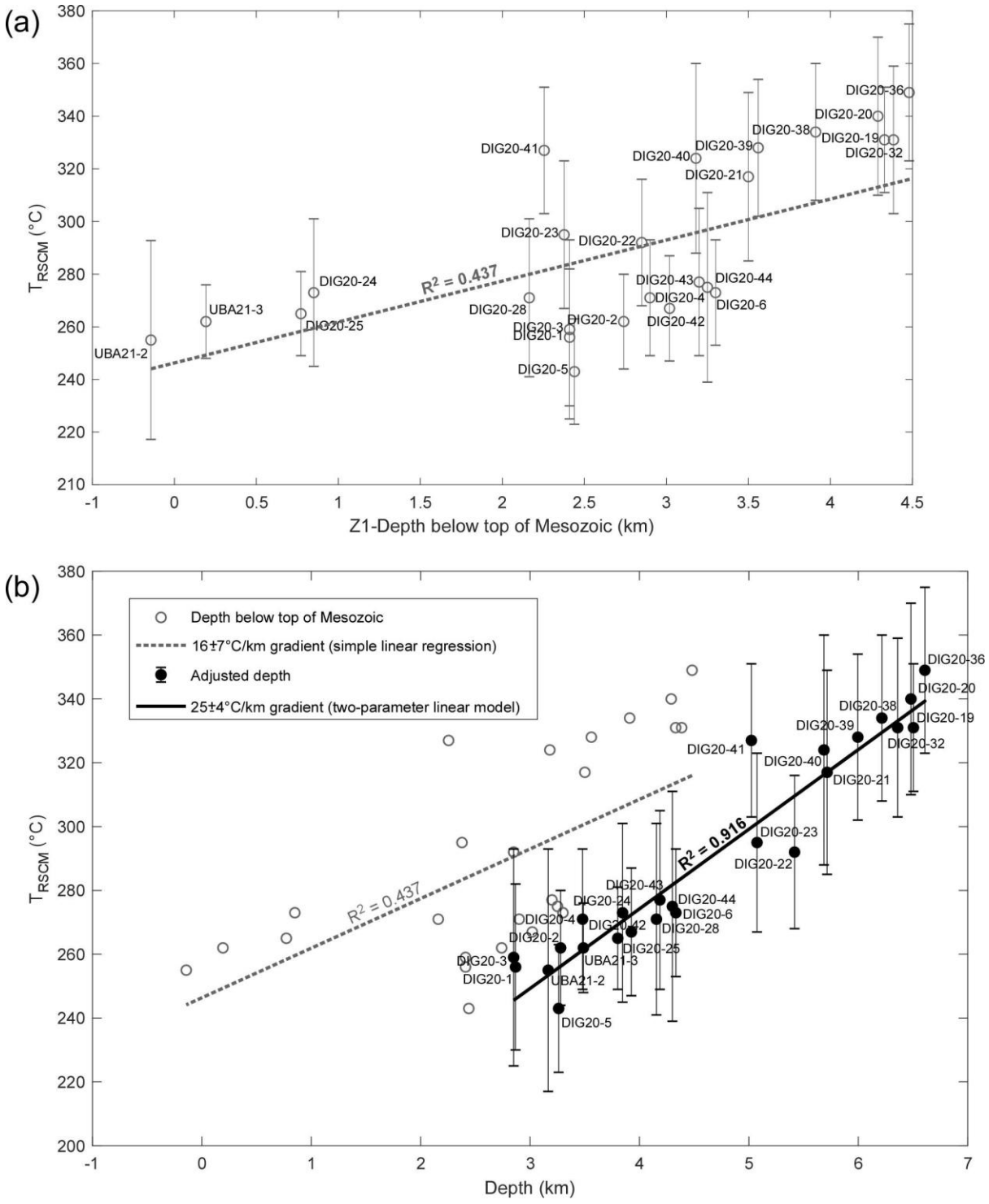
(a)
T_RSCM (°C)
Z1-Depth below top of Mesozoic (km)
R² = 0.437
DIG20-36
DIG20-20
DIG20-38
DIG20-19
DIG20-32
DIG20-41
DIG20-39
DIG20-40
DIG20-21
DIG20-23
DIG20-22
DIG20-24
DIG20-43
DIG20-44
DIG20-4
DIG20-6
UBA21-3
DIG20-28
DIG20-2
DIG20-42
DIG20-25
DIG20-3
DIG20-1
UBA21-2
DIG20-5
(b)
Depth below top of Mesozoic
16±7°C/km gradient (simple linear regression)
Adjusted depth
25±4°C/km gradient (two-parameter linear model)
T_RSCM (°C)
Depth (km)
R² = 0.437
R² = 0.916
DIG20-36
DIG20-20
DIG20-38
DIG20-19
DIG20-39
DIG20-32
DIG20-41
DIG20-40
DIG20-21
DIG20-23
DIG20-22
DIG20-43
DIG20-24
DIG20-44
DIG20-4
DIG20-6
DIG20-2
DIG20-28
DIG20-25
UBA21-3
DIG20-3
DIG20-1
UBA21-2
DIG20-5

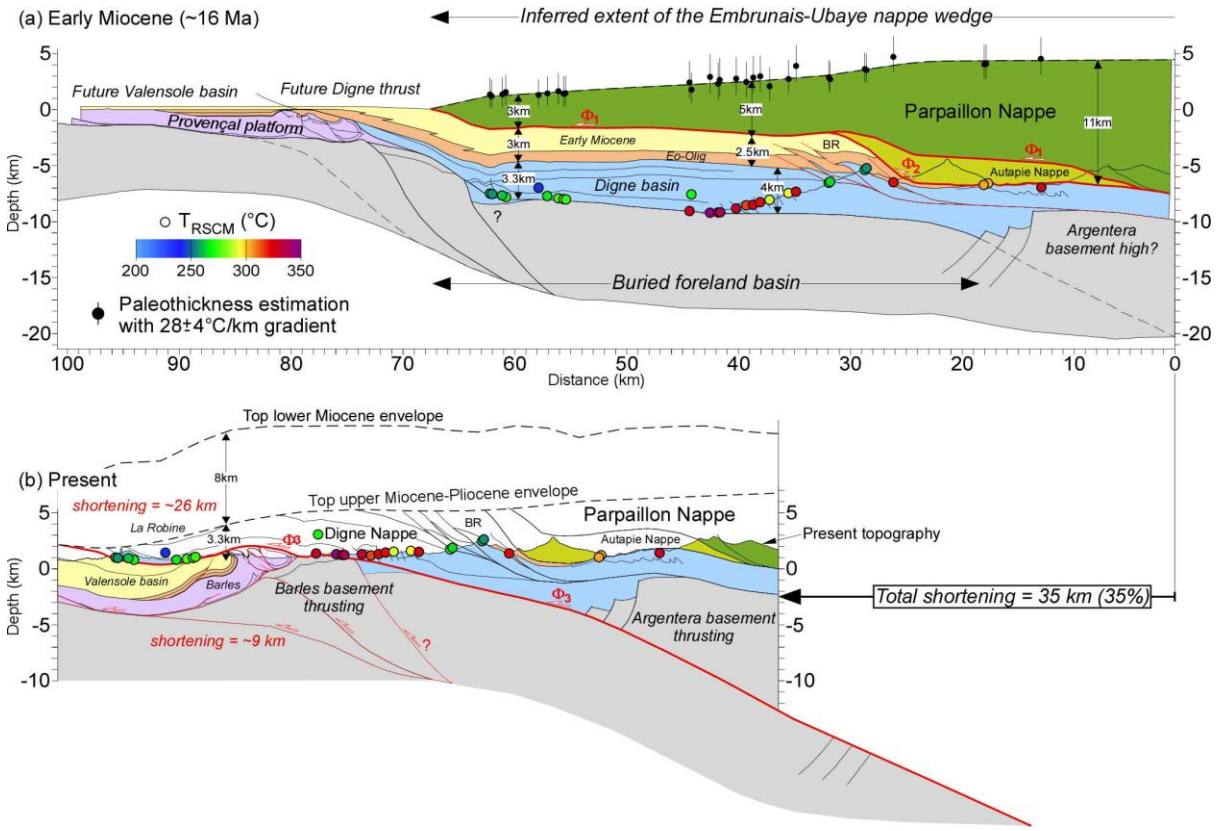
(a) Early Miocene (~16 Ma)
Inferred extent of the Embrunais-Ubaye nappe wedge
Future Valensole basin
Future Digne thrust
Provençal platform
Parpaillon Nappe
Early Miocene
Eo-Olig
Digne basin
Autapie Nappe
Argentera basement high?
Buried foreland basin
T_RSCM (°C)
200 250 300 350
Paleothickness estimation with 28±4°C/km gradient
Depth (km)
Distance (km)
(b) Present
Top lower Miocene envelope
Top upper Miocene-Pliocene envelope
shortening = ~26 km
La Robine
Digne Nappe
Present topography
Total shortening = 35 km (35%)
Valensole basin
Barles
Barles basement thrusting
Argentera basement thrusting
shortening = ~9 km

Sample label (from SW to NE)	Latitude	Longitude	Elevation (m)	Stratigraphic age	Number of spectra	RA1 parameter		T_{RSCM} (°C)			D1 (km)	Z1 (km)	T_{RSCM} modeled (°C)	SD 95%CI (°C)	T misfit (°C)	Z adjusted (km)	Paleodepth (km)		
						Mean	SD	Mean	SD	SE							24°C/km	28°C/km	32°C/km
DIG20-3	44.107908	6.207417	1002	Hettangian	12	0.584	0.013	259	17	5	5.13	2.41	245.53	8.16	13.47	2.85	10.38	8.89	7.78
DIG20-1	44.089290	6.237561	614	Rhaetian	19	0.581	0.010	256	13	3	5.33	2.41	245.96	8.10	10.04	2.87	10.25	8.79	7.69
DIG20-2	44.091327	6.244497	619	Hettangian	20	0.585	0.007	262	9	2	6.28	2.74	256.23	7.31	5.77	3.28	10.50	9.00	7.88
DIG20-4	44.119019	6.233895	634	Sinemurian	20	0.593	0.008	271	11	2	6.76	2.9	261.25	6.99	9.75	3.48	10.88	9.32	8.16
DIG20-5	44.161286	6.238802	690	Pliensbachian	19	0.570	0.008	243	10	2	9.57	2.44	255.78	6.64	-12.78	3.26	9.71	8.32	7.28
DIG20-42	44.178098	6.215883	815	Pliensbachian	13	0.589	0.008	267	10	3	10.56	3.02	272.37	5.80	-5.37	3.92	10.71	9.18	8.03
DIG20-43	44.187951	6.215586	875	Sinemurian	14	0.598	0.011	277	14	4	11.50	3.2	278.87	5.54	-1.87	4.19	11.13	9.54	8.34
DIG20-6	44.175673	6.256877	718	Hettangian	20	0.594	0.007	273	10	2	12.04	3.3	282.52	5.46	-9.52	4.33	10.96	9.39	8.22
DIG20-44	44.194490	6.214926	908	Rhaetian	10	0.596	0.014	275	18	5	12.25	3.25	281.72	5.39	-6.72	4.30	11.04	9.46	8.28
DIG20-32	44.265851	6.295359	1290	Rhaetian	10	0.642	0.011	331	14	4	23.02	4.38	333.09	7.75	-2.09	6.36	13.38	11.46	10.03
DIG20-28	44.227906	6.361812	1005	Aalenian-Bajocian	13	0.593	0.012	271	15	4	23.26	2.16	278.08	4.16	-7.08	4.15	10.88	9.32	8.16
DIG20-36	44.284355	6.306348	1135	Sinemurian	15	0.656	0.010	349	13	3	24.81	4.48	339.29	8.38	9.71	6.61	14.13	12.11	10.59
DIG20-19	44.270791	6.315185	1120	Rhaetian	20	0.642	0.008	331	10	2	25.35	4.33	336.70	8.04	-5.70	6.50	13.38	11.46	10.03
DIG20-20	44.264198	6.331582	1133	Hettangian	17	0.650	0.012	340	15	4	25.55	4.29	336.13	7.96	3.87	6.48	13.75	11.79	10.31
DIG20-38	44.307058	6.322171	1258	Hettangian	12	0.645	0.010	334	13	4	26.88	3.91	329.49	7.16	4.51	6.21	13.50	11.57	10.13
DIG20-21	44.267387	6.369224	1175	Toarcian	10	0.623	0.028	317	16	5	25.83	3.5	317.02	5.85	-0.02	5.71	12.79	10.96	9.59
DIG20-39	44.317887	6.328232	1329	Toarcian	12	0.640	0.010	328	13	4	28.40	3.56	324.01	6.58	3.99	5.99	13.25	11.36	9.94
DIG20-40	44.329833	6.328552	1449	Aalenian	10	0.636	0.015	324	18	6	29.22	3.18	316.28	5.89	7.72	5.68	13.08	11.21	9.81
DIG20-22	44.296487	6.396662	1271	Bajocian	19	0.610	0.010	292	12	3	29.93	2.85	309.57	5.43	-17.57	5.42	11.75	10.07	8.81
DIG20-23	44.301576	6.400749	1293	Bajocian	18	0.613	0.011	295	14	3	31.45	2.38	301.02	5.20	-6.02	5.07	11.88	10.18	8.91
DIG20-41	44.353453	6.361389	1279	Bajocian	15	0.639	0.010	327	12	3	32.27	2.25	299.73	5.31	27.27	5.02	13.21	11.32	9.91
DIG20-24	44.320107	6.428385	1540	Tithonian	19	0.593	0.011	273	14	3	34.93	8.5	270.36	6.71	2.64	3.84	10.96	9.39	8.22
DIG20-25	44.321007	6.430626	1558	Early Cretaceous	18	0.588	0.006	265	8	2	35.32	0.77	269.25	6.89	-4.25	3.80	10.63	9.11	7.97
UBA21-3	44.380740	6.395494	1994	Late Cretaceous	15	0.585	0.006	262	7	2	38.42	0.19	261.44	8.35	0.56	3.49	10.50	9.00	7.88
UBA21-2	44.383208	6.398964	2112	Late Eocene	14	0.579	0.016	255	19	5	38.59	-0.14	253.42	9.10	1.58	3.17	10.21	8.75	7.66
UBA20-1	44.458186	6.378825	800	Tithonian	15	0.652	0.009	343	11	3	-	-	-	-	-	-	13.88	11.89	10.41
UBA21-6B	44.437839	6.417384	905	Late Cretaceous	15	0.638	0.011	326	14	4	-	-	-	-	-	-	13.17	11.29	9.88
UBA21-6A	44.437839	6.417384	906	Late Eocene	17	0.639	0.007	328	8	2	-	-	-	-	-	-	13.25	11.36	9.94
UBA20-4	44.373340	6.457446	1410	Early Oligocene	13	0.636	0.013	324	16	4	-	-	-	-	-	-	13.08	11.21	9.81
UBA20-2	44.448027	6.411324	877	Early Oligocene	15	0.630	0.012	319	11	3	-	-	-	-	-	-	12.88	11.04	9.66
UBA20-7	44.398928	6.533754	1077	Callovian-Oxfordian	15	0.621	0.005	306	6	2	-	-	-	-	-	-	12.33	10.57	9.25
UBA20-10	44.386518	6.563662	1156	Callovian-Oxfordian	15	0.620	0.007	304	9	2	-	-	-	-	-	-	12.25	10.50	9.19
UBA20-8	44.413045	6.619639	1415	Callovian-Oxfordian	13	0.643	0.008	332	10	3	-	-	-	-	-	-	13.42	11.50	10.06
UBA21-5	44.360419	6.785619	2076	Early Oligocene	15	0.601	0.009	281	11	3	-	-	-	-	-	-	11.29	9.68	8.21